

1 **A multiple dating-method approach applied to the**
2 **Sanabria Lake moraine complex (NW Iberian Peninsula,**
3 **SW Europe)**

4 **Laura Rodríguez-Rodríguez^a, Montserrat Jiménez-Sánchez^a, María José Domínguez-**
5 **Cuesta^a, Vincent Rinterknecht^b, Raimon Pallàs^c, Didier Bourlès^d, Blas Valero-Garcés^e**

6 *^aDpto. Geología, Universidad de Oviedo, Arias de Velasco s/n, 33005 Oviedo, Spain*

7 *laurarr@geol.uniovi.es; +34 985102936 (corresponding author)*

8 *^bDepartment of Earth and Environmental Sciences, University of St Andrews, Fife KY16*

9 *9AL, UK*

10 *^cDept. Geodinàmica i Geofísica, Universitat de Barcelona, 08028 Barcelona, Spain*

11 *^dAix Marseille Université, CNRS-IRD-Collège de France, UM34 CEREGE, 13545 Aix-en-*

12 *Provence, France*

13 *^eIPE-CSIC, Avda. Montañana 1005, 50059 Zaragoza, Spain*

14 **Abstract**

15 New evidence in the NW region of the Iberian Peninsula (~42°N 6°W) of a glacial advance
16 coeval with the global Last Glacial Maximum (LGM) of the Marine Isotope Stage 2 has
17 been identified through a dataset of exposure ages based on $^{23}\text{^{10}Be}$ concentration
18 measurements carried out on boulder samples taken from a set of latero-frontal moraines.
19 Results span the interval 19.2–15.4 ^{10}Be ka, matching the last deglaciation period when
20 Iberia experienced the coldest and driest conditions of the last 25 ka, and are consistent
21 with Lateglacial chronologies established in other mountain regions from SW Europe. The
22 extent of the LGM stade identified in this work is similar to the local maximum ice extent
23 stade recorded and dated as prior to 33 ka using radiocarbon and optically stimulated
24 luminescence. This work showcases how multiple-dating approaches and detailed
25 geomorphological mapping are required to reconstruct realistic palaeoglacier evolution
26 models.

27 **Key words**

28 Cosmogenic dating, glacial geomorphology, ice cap, Last Glacial Maximum, Lateglacial,
29 Sanabria, Iberian Peninsula.

30 **1. Introduction**

31 Evidence for asynchronism between the maximum advances of mountain glaciers and
32 continental ice sheets is reported worldwide, suggesting that the dynamics of both ice
33 systems responded differently to rapid changes in temperature and/or moisture supply (e.g.
34 Gillespie and Molnar, 1995; Florineth and Schlüchter, 2000; Zreda et al., 2011). Ice sheets
35 grew to their maximum position between 33 and 26.5 ka in response to climatic forcing
36 from decreases in summer insolation, tropical Pacific sea surface temperatures and
37 atmospheric CO_2 levels, and nearly all were at their Last Glacial Maximum (LGM)

38 positions from 26.5 to 19-20 ka corresponding to minima in these forcings (Clark et al.,
39 2009). The latter implies a longer time interval for the LGM episode than previous
40 estimations based on the marine isotope and global sea level records (18 ¹⁴C ka BP or 21 ka
41 cal BP; Ehlers and Gibbard, 2007). Regional differences in maximum ice extent (Würmian
42 MIE) and timing between mountain regions and the asynchrony with the global LGM hold
43 significant information on cryosphere dynamics and palaeoclimatic evolution during the
44 last glacial cycle. In the mountain regions of southern Europe, two chronological scenarios
45 were proposed (Hughes and Woodward, 2008): (1) a local glacial maximum several
46 thousands of years earlier than the LGM of Marine Isotope Stage 2 (MIS 2) based on
47 evidence from northern Iberian Peninsula, Italian Apennines and Greece dated with
48 radiocarbon, Uranium series, and optically stimulated luminescence (OSL) techniques, and
49 (2) a local glacial maximum close or coeval with the global LGM based on evidence from
50 central Iberian Peninsula, Pyrenees, Maritime Alps and Turkey dated through terrestrial
51 cosmogenic nuclides (TCN). Such contrasting scenarios could be related to regional climate
52 variability, but also to limitations or biases of the applied dating methods, as TCN methods
53 consistently provided the youngest ages and radiocarbon and OSL the oldest ones (Hughes
54 and Woodward, 2008).

55 In the Iberian Peninsula mountains (Figure 1), the current knowledge about the extent,
56 timing and number of glacial stades during the last glacial cycle (ca. last 120 ka) has been
57 recently reviewed (Calvet et al., 2011; Jiménez-Sánchez et al., 2013) and is summarized as
58 follows: (1) in the Pyrenees the Würmian MIE occurred between 97 and 36 ka depending
59 on the valleys considered (García-Ruiz et al., 2013; Lewis et al., 2009; Pallàs et al., 2010),
60 in the Cantabrian Mountains it was prior to 38 ka (Jalut et al., 2010; Jiménez-Sánchez and
61 Farias, 2002; Moreno et al., 2010; Serrano et al., 2012, 2013), and in the Sistema Central

62 occurred between 33-26 ka (Carrasco et al., 2013; Palacios et al., 2010, 2012; Vieira,
63 2008); (2) a new glacial advance took place during the LGM recording a glacial advance
64 similar in extent to previous local MIE in the eastern end of the southern Pyrenees (23-21
65 ka) (Delmas et al., 2008; Pallàs et al., 2006, 2010) and in the Sistema Central (22-19 ka)
66 (Carrasco et al., 2013; Palacios et al., 2010, 2012) while shorter glacial advances were
67 recorded in the northern Pyrenees (20-18 ka) (Delmas et al., 2011), the western end of the
68 southern Pyrenees (García Ruiz et al., 2003; Lewis et al., 2009), and the Cantabrian
69 Mountains (almost ice-free conditions in some valleys by 20 ka) (Jiménez-Sánchez and
70 Farias, 2002); (3) frontal moraines coeval with the Oldest Dryas have been dated in the
71 eastern Pyrenees and in the Sistema Central (Delmas et al., 2009; 2011; Pallàs et al., 2006,
72 2010; Palacios et al., 2010, 2012). In spite of all these new datasets, it remains unclear to
73 what extent the differences in magnitude between local Würmian MIE and LGM stades
74 might result from biases introduced by regional climate patterns, the dating methods, or
75 even from uncertainties in the interpretation of the feature being dated. The latter can be
76 particularly significant for glacial sequences composed of till deposits arranged as sets of
77 frontal moraines, since depending on their preservation they can be interpreted as resulting
78 from: (i) a single glaciation or episode of glacial advance and retreat with deposition of
79 recessional moraines close in age, or (ii) more than one glaciation with superimposed
80 glacial records. In the last case the moraines forming the frontal moraine complex would be
81 very different in age.

82 The Sanabria Lake moraine complex provides a unique glacier setting in the Iberian
83 Peninsula to test these hypotheses. The occurrence of a well-preserved glacial sequence that
84 includes a set of recessional moraines with related glaciolacustrine successions, allowed the
85 combination of geomorphological techniques with several dating methods to establish the

86 significance of the whole moraine complex. The aims of this paper are 1) to constrain the
87 timing and extent of glaciers during the last glacial cycle by combining new moraine ^{10}Be
88 surface exposure ages with the pre-existing ^{14}C and OSL datasets, 2) to discuss the
89 relevance of the new local chronology, by comparing it with other palaeoclimate records of
90 Iberia and SW Europe.

91 **2. Regional Setting**

92 The Sanabria Lake area in NW Iberian Peninsula is located in the east side of the Trevinca
93 Massif, a mid-latitude mountain range which is free of ice at present (Figure 1). The massif
94 highlands are characterized by a smooth topographic plateau reaching an altitude of 2128
95 m. The northern rim of the plateau is cut by north-facing glacial cirques, which connect
96 with Alpine glacial valleys up to 7 km-long. To the south the plateau decreases in height
97 and slope progressively to c. 1600 m, where two main troughs, the Bibei and Tera valleys
98 are incised. These glacial valleys are 26 km and 23.5 km-long, and drain W and E
99 respectively. Additionally, the plateau area is drained by minor glacial valleys arranged in a
100 radial pattern (Figure 1).

101 An ice cap covered the plateau during the local MIE, lowering the equilibrium line altitude
102 to 1687 m in the Tera outlet (Cowton et al., 2009). Moraine deposits can be divided into
103 two groups according to their distribution: (i) moraine complexes below 1600 m marking
104 the terminal zones of the glacial valleys, and (ii) cirque moraines at altitudes above 1700 m.
105 We focus on an area of 45 km² in the terminal zone of the former Tera glacial outlet, where
106 a moraine complex and ice-related deposits are particularly well-preserved around the
107 Sanabria Lake (Figures 1 and 2). It includes: (i) a system of lateral moraines longer than 6
108 km that connects to the front with undifferentiated tills delineating the local MIE and (ii)
109 remains of at least nine frontal moraines spreading over a distance of 2 km. Directly up-

110 valley from this moraine complex, a 9 m-long sediment core retrieved from the deepest part
111 of the Sanabria Lake shows a 1.8 m-thick basal unit with massive sands to banded silts and
112 clays dated by ^{14}C AMS between 25.6 ± 0.4 and 14.5 ± 0.3 cal yr BP (Rodríguez-Rodríguez
113 et al., 2011). Considering a proglacial origin for these facies, the frontal recessional
114 moraine enclosing the lake must be older than the basal age of the lake and consequently,
115 some of the moraines could represent different positions of the glacier front during the post-
116 MIE glacial retreat prior to 25.6 ka. A > 12 m-long core from the San Martín ice-dammed
117 deposit located out with the outermost left lateral moraine and interpreted as synchronous
118 or subsequent to the local MIE, gives a minimum age of 21.8 ± 0.4 cal yr BP (Rodríguez-
119 Rodríguez et al., 2011). Published radiocarbon ages obtained from other cores from small
120 ponds in the eastern side of the Trevinca Massif also constrain minimum ages for local
121 glacier retreat (Figure 2): (i) 15.7 ± 0.4 cal yr BP at Laguna de La Roya (Allen et al., 1996;
122 Muñoz-Sobrino et al., 2013); (ii) 18.1 ± 0.4 cal yr BP at Laguna de las Sanguijuelas
123 (Muñoz-Sobrino et al., 2004) and (iii) 14.2 ± 0.3 cal yr BP at Lleguna (Allen et al., 1996).
124 Additional time constraints is provided by Pias site, in the western side of the Trevinca
125 Massif, where a sedimentary sequence composed of fine-grained lacustrine deposits lying
126 on poorly sorted sandy gravels interstratified with massive diamicton layers is well-
127 preserved at the junction between the Bibei and Barxacoba glacial valleys. Three quartz
128 samples retrieved from glacio-fluvial and glacio-lacustrine sand units less than 1-m thick
129 were analyzed with OSL and yielded minimum ages of 27 ± 2 ka, 31 ± 3 ka, and 33 ± 3 ka
130 for the regional MIE (Pérez-Alberti et al., 2011). Based on this information, we identify
131 two groups of chronological data post-dating the local MIE in the Trevinca Massif: (i)
132 previous to the LGM (OSL dates) and (ii) synchronous or younger than the LGM
133 (radiocarbon dates, Table 1).

134 **3. Methodology**

135 A geomorphological map (at a 1:50.000 scale) was produced through photointerpretation
136 and was used to reconstruct the MIE of local glaciers in the whole massif by using an
137 ArcGIS database (v. 9.2) and the spreadsheet Profiler v.2 (Benn and Hulton, 2010). Ice
138 profiles were numerically modeled along 31 profiles disposed radially from the ice cap
139 margin to its source area along its outlet glaciers.

140 The TCN analysis was conducted in the Sanabria Lake moraine complex, where the
141 outermost lateral moraines were presumably formed during the local Würmian MIE stade,
142 while the inset ones recorded subsequent post-MIE ice front locations (Figures 1 and 2).

143 We selected 23 samples to investigate the minimum surface exposure age for the end of the
144 Würmian MIE stade and for three other subsequent glacial fronts. The sampling selection
145 was designed considering the relative chronology of the moraine complex to cover as
146 complete as possible the history of the Pleistocene glaciations in the Tera Valley (eastern
147 side of the Trevinca Massif). A total number of five moraines were sampled, two of them
148 (TER and MAR) corresponding to the left lateral moraine which marks the local MIE (a
149 total of eight boulders) and the others (SAN, TET and SAU) corresponding to three
150 subsequent glacial fronts (five boulders each one). The shielding effect of till or snow
151 cover, the underexposure of moraine boulders and the tilting of boulder surfaces was
152 minimized by choosing only those boulders lying at the top of the crest and showing the
153 largest size (volume greater than a cubic meter or $> 1 \text{ m}^3$), a well anchored base (but
154 protruding at least 1 m from the moraine surface), and a flat surface (table-type). The
155 crystalline character of the bedrock in the Tera catchment, which is mainly composed of
156 augen gneiss with quartz-rich streaks and granodiorites with quartz-rich veins up to 6 cm-
157 thick, allowed getting samples very riched in quartz directly in the field. Shallow samples

158 were taken manually with hammer and chisel. Angular elevation of the horizon was
159 measured at each sampling site with a clinometer and the topographic shielding factors was
160 calculated using the CRONUS-Earth calculator (version 1.1.) following Balco et al. (2008).
161 The sample treatment was performed in the *Laboratori de Cosmonúclids Terrestres de la*
162 *Universitat de Barcelona* (Spain). Samples were crushed and sieved to obtain the 0.25-1
163 mm grain fraction. Other mineral phases except quartz were removed from the samples by
164 magnetic separation (dark minerals), froth floatation (mainly feldspars), and repeated
165 leaching (Kohl and Nishiizumi, 1992). Aluminum content was analyzed through ICP-OES
166 on sample aliquots at the *Centre Científic i Tecnològic de la Universitat de Barcelona*
167 (CCiTUB). The aluminum content in all samples is < 250 ppm to ensure an efficient
168 separation of Be and Al during column chromatography. Muscovite grains were removed
169 through sample shaking with clean paper sheets and 3 extra acid-batches in order to reduce
170 the Al-content in samples SAU01, MAR03 and SAN05. For each sample between 14-23 g
171 of clean quartz grains were spiked with 200 mg of ^9Be carrier and completely digested in
172 48% HF. The carrier used was a commercial standard solution 1000 mg/l of beryllium
173 oxide in hydrochloric acid 2% from the Scharlau Company (1.02g/cm^3). Beryllium fraction
174 of each sample was extracted through column chromatography (Ditchburn and Whitehead,
175 1994).
176 All the ^{10}Be concentration measurements were performed at the ASTER AMS facility in
177 Aix-en-Provence, France. The measured $^{10}\text{Be}/^9\text{Be}$ ratios were corrected for lab procedural
178 blanks and calibrated with the NIST_27900 beryllium standard (Reference Material 4325,
179 assigned value of $2.79 \pm 0.03 \times 10^{-11}$) and using a ^{10}Be half-life of $1.36 \pm 0.07 \times 10^6$ years
180 (Nishiizumi et al., 2007). Analytical uncertainties are reported as 1σ and include
181 uncertainties associated with AMS counting statistics, standard uncertainty (certification),

182 and chemical blank measurements. ^{10}Be concentration in quartz samples (Tables 2 to 4)
183 was calculated following Balco (2006), while the surface exposure ages were calculated
184 with the Cronus online calculator v. 2.2.1 assuming no erosion (Balco et al., 2008; Balco,
185 2010). Maximum erosion rates were estimated by calculating the ratio between the height
186 of protruding minerals from boulder surfaces and the corresponding exposure ages deduced
187 for no erosion. Correcting exposure ages using the maximum erosion rate of $6.66 \times 10^{-5} \text{ cm}$
188 yr^{-1} yielded exposure ages older by only ~ 200 years. Boulder ages discussed in this work
189 were not corrected for erosion nor snow/vegetation cover to ensure that the reported ages
190 are treated as minimum exposure ages. Moraine ages were obtained as the error-weighted
191 mean of the exposure ages calculated for its boulders in the constant production rate model.
192 Only the oldest boulders of each moraine, whose exposure ages are overlapping at 1σ , were
193 used to derive the error-weighted mean moraine ages (Figure 3): (i) TER-02, TER-05,
194 MAR-03 for the TER-MAR moraine; (ii) SAN-02, SAN-04, SAN-05 for the SAN moraine;
195 (iii) TET-01, TET-02, TET-03 for the TET moraine; and (iv) SAU-01, SAU-02 SAU-04
196 for the SAU moraine. This TCN chronology is compared with pre-existing OSL and ^{14}C
197 datasets in the discussion.

198 **4. Results**

199 The geomorphological map (Figure 1) summarizes the main glacial evidence on the
200 Trevinca Massif and its relative chronology, allowing the reconstruction of the ice cap
201 dimensions. Ice fronts reached altitudes between 1580 – 950 m, 1510 – 1110 m, 1290 – 980
202 m, and 1170 – 1060 m in the East, North, West and South sides of the massif, respectively.
203 The lowest altitudes correspond to the Tera and Bibei valleys, where the glacial front
204 fluctuations left remarkable sets of moraines. According to the ice surface model, glaciers
205 extended 475 km^2 over the massif during the local MIE, reaching up to 200 m of ice

206 thickness on the plateau and up to 450 m in the glacial valleys. The Sanabria Lake moraine
207 complex indicates that the glacier outlet that flowed along the Tera valley was 23.5 km long
208 during the local MIE and recorded a total length reduction of 3 km by the time of the SAU
209 moraine deposition. The width of this glacier tongue, measured at the eastern part of the
210 Sanabria Lake basin, changed from 3.7 km to 1.7 km between the local MIE and the SAU
211 stade, while the ice thickness reduced ca. 130 m according to ice surface estimations made
212 in the Tera Valley using the spreadsheet Profiler v.2 (Benn and Hulton, 2010).

213 A minimum age of 19.2 ± 1.8 ^{10}Be ka ($n = 3$) can be established for the gently sloped left
214 lateral moraine (TER-MAR) (Figures 2 to 4; Tables 3 and 4). The SAN frontal moraine
215 marks a subsequent glacial still stand or minor readvance no later than 17.7 ± 1.7 ^{10}Be ka (n
216 $= 3$). The minimum age for the TET moraine, located in a small tributary of the main Tera
217 Valley, suggests the lack of connection between glacier streams of both valleys by $17.2 \pm$
218 1.6 ^{10}Be ka ago ($n = 3$). Meanwhile, the overall retreating Tera ice front located downwards
219 from the Sanabria over-deepened depression (today occupied by the Sanabria Lake)
220 deposited another five frontal moraines. We report a minimum age of 15.7 ± 1.5 ^{10}Be ka (n
221 $= 3$) for the SAU moraine, which dams modern day Sanabria Lake.

222 The lack of geomorphological features indicating the location of the ice margins at higher
223 elevations than the TET moraine does not allow establishing a detailed paleogeographic
224 model for each subsequent deglaciation stade.

225 **5. Discussion**

226 The minimum ^{10}Be ages cover the time interval 19.2 ± 1.8 to 15.7 ± 1.5 ^{10}Be ka
227 (uncertainties include those associated with the analytical procedures and the production
228 rate) and are consistent with the relative chronology derived from the geomorphological
229 sequence (Figure 2). Combining the new ^{10}Be dataset with published ^{14}C AMS and OSL

230 results from the whole massif, we have identified two glacial advances very close in extent.
231 The oldest one is recorded by glacio-fluvial sediments at Pias site (western Trevinca
232 Massif) which yielded OSL ages $\sim 27\text{--}33$ ka (Pérez-Alberti et al., 2011), suggesting the
233 occurrence of a local MIE earlier than MIS 2. The youngest one is supported by our TCN
234 results. According to the new set of minimum ^{10}Be ages, the whole moraine sequence was
235 developed between $19.2\text{--}15.7$ ka (Figure 2). The outermost TER-MAR lateral moraine
236 yields a minimum age of 19.2 ± 1.8 ^{10}Be ka for the glacier retreat; the minimum age for the
237 sedimentation onset in the San Martín valley (as a consequence of the moraine runoff
238 blockage) was radiocarbon-dated as 21.8 ± 0.4 cal ka BP (Rodríguez-Rodríguez et al.,
239 2011). Both minimum ages are consistent with a second glacial advance during the LGM of
240 MIS 2 very close in extent to the previous MIE. The SAN moraine, located in a retreated
241 position compared with the TER-MAR moraine, was dated at 17.7 ± 1.7 ^{10}Be ka, which is
242 consistent with the minimum ^{14}C AMS age of 18.1 ± 0.4 cal ka BP obtained from Laguna
243 de las Sanguijuelas located between both moraines (Muñoz-Sobrino et al., 2004) (Figure 2).
244 The TET moraine was deposited shortly after, at a minimum age of 17.2 ± 1.6 ^{10}Be ka,
245 marking the separation between the main Tera glacier and its eastern tributary. Between
246 17.7 and 15.7 ^{10}Be ka, the retreating ice front built up five frontal moraines. The SAU
247 moraine damming the Sanabria Lake represents the youngest frontal moraine of this
248 sequence and yields a minimum exposure age of 15.7 ± 1.5 ^{10}Be ka. The consistence
249 between ages obtained from the boulders in each moraine and published radiocarbon data
250 suggests that the ^{10}Be results are not significantly affected by moraine post-depositional
251 erosion in this area.
252 The ^{14}C AMS age of 15.7 ± 0.4 cal yr BP obtained at the base of the lacustrine deposit
253 known as Laguna La Roya, located at 1608 m altitude next to the eastern plateau edge,

254 suggests that at least the southern part of the plateau could have been partly ice-free by the
255 time of the SAU moraine deposition (Allen et al., 1996; Muñoz-Sobrino et al., 2013; Figure
256 2). This hypothesis is coherent with an ELA rising of about 100-150 m compared to the
257 local MIE, which would have caused a drastic reduction (by more than 80 %) in the extent
258 of the accumulation zone in the southern part of the plateau. Therefore, the ice flow inputs
259 from the Segundera-Cárdena valley would have been reduced and the ice source area would
260 have been located in the northern part of the Tera catchment where the plateau records its
261 highest elevation (Figure 1). The basal ^{14}C AMS ages obtained at the Lleguna core ($14.2 \pm$
262 0.3 cal yr BP; Allen et al., 1996) and at the top of the basal detrital unit of the Sanabria
263 Lake core (14.5 ± 0.3 cal yr BP; Rodríguez-Rodríguez et al., 2011) would represent the
264 timing of glacial front retreat from the eastern part of the Sanabria Lake.

265 We note that the new ^{10}Be ages and the published ^{14}C AMS dataset are generally consistent,
266 but one question remains concerning the disparity between the minimum ages obtained for
267 the base of the Sanabria Lake sequence (25.6 ka cal BP), the San Martín ice dammed
268 deposit (21.8 ka cal BP) (Rodríguez-Rodríguez et al., 2011) and the TER-MAR lateral
269 moraine (19.2 ^{10}Be ka) reported in this work. The Sanabria Lake sequence is considerably
270 older than the TER-MAR moraine and its associated ice dammed deposit. A possible
271 explanation is a local LGM stade (prior to 21.8 ka) advancing over the Sanabria Lake basin
272 and eroding the upper part of the sedimentary sequence related to the previous Würmian
273 MIE retreat (~33 ka). Although ice-push structures (folding, faults) were not found in the
274 basal unit of the Sanabria core, the occurrence of iron oxide-rich intervals could suggest a
275 sedimentary unconformity, otherwise difficult to identify in the massive sandy levels.
276 Alternatively, basal ages of the Sanabria Lake and San Martín sequences (derived from
277 bulk sediment samples) could be older than the enclosing sediments if any reworking had

278 happened or if considerable reservoir effects had taken place. However, the consistence
279 between the ^{14}C AMS data obtained from these sequences and the OSL ages obtained in the
280 Pias site at the western side of the massif suggests that this is not likely to be the case.
281 There is a strong coherence between the Sanabria dataset and other mountain regions in the
282 Iberian Peninsula. The Würmian MIE stade observed in the Sanabria area (prior to 33 ka)
283 correlates with a similar stade documented in the Sistema Central ~ 200 km southwards
284 (33-26 ka) (Carrasco et al., 2013; Domínguez-Villar et al., in press; Palacios et al., 2010,
285 2012; Vieira, 2008), but is younger than the one recorded in the Cantabrian Mountains ~
286 100 km northwards (prior to 38 ka) (Jalut et al., 2010; Jiménez-Sánchez and Farias, 2002;
287 Moreno et al., 2010; Serrano et al., 2012, 2013) and in the Pyrenees ~ 450 km
288 northeastwards (97-36 ka) (García-Ruiz et al., 2013; Lewis et al., 2009; Pallàs et al., 2010;
289 Peña et al., 2004). According to multi-proxy reconstructions based on Iberian lacustrine and
290 marine records, cold and relatively wet conditions during the MIS 5 to MIS 4 transition
291 were responsible for the MIE of glaciers, at least, in northern Iberia; a shift towards greater
292 aridity during MIS 4 and MIS 3 would have been responsible for subsequent deglaciation
293 (Moreno et al., 2012). The mountain glacial advance during the global LGM has also been
294 recorded differently across Iberia, reaching quasi-MIE positions not only in Sanabria, but
295 also in the eastern part of the southern Pyrenees (Pallàs et al., 2006, 2010; Delmas et al.,
296 2008) or the Sistema Central (Carrasco et al., 2013; Palacios et al., 2010, 2012). In other
297 areas, like the Cantabrian Mountains or the northern and southwestern Pyrenees, the glacial
298 advance was clearly less extensive (e.g. Jiménez-Sánchez et al., 2013; Delmas et al., 2011).
299 Subsequent glacial retreat in Sanabria started no later than 19.2 ^{10}Be ka and recorded
300 several glacial front stabilizations until 15.7 ^{10}Be ka. This glacier evolution is consistent
301 with palaeoclimate reconstructions based on speleothem and lacustrine sequences from the

302 Iberian Peninsula which indicate that the coldest and driest interval of the last 25 ka took
303 place between 18.2 and 15.4 ka (Moreno et al., 2012) during the Lateglacial, coinciding
304 with the Mystery Interval, a stadial that occurred during the earliest phase of the last
305 deglaciation (17.5 to 14.5 cal ka BP) coevally with low boreal summer and high austral
306 summer insolation and with low temperatures in Greenland (HE1) (Denton et al., 2005,
307 2006).

308 The Sanabria dataset is also coherent with glacial evidence from other mid-latitude
309 mountains across SW Europe. In the Alps, the Late Würmian glaciation reached the Alpine
310 lowlands between 30 ka and 21 ka and was followed by a series of glacial front
311 stabilizations between 18 – 17 ka to 14.7 ka and 11.3 to 9.7 ka (Darnault et al., 2012; Ivy-
312 Ochs et al., 2008 and references therein). In the Tatra Mountains (western Carpathians),
313 three trimlines have been identified and constrained with cosmogenic isotope ^{36}Cl revealing
314 that a post-LGM glacial retreat started no later than 21.5 ka and subsequent glacial
315 advances occurred at ~ 17 and 12 ka (Makos et al., 2013). Minimum moraine ages based on
316 U-Th analysis, carried out in secondary calcite cements, and thermo luminescence (TL)
317 analysis obtained from glacio-fluvial sediments in the Pindus Mountains supported a LGM
318 advance of glaciers considerably less extensive than other glacial advances associated to
319 previous cold stages (MIS 6 and MIS 12) in northwestern Greece (Hughes et al., 2006;
320 Woodward et al., 1995, 2008). Similar U-Th studies in the Montenegro Mountains (Dinaric
321 Alps) also revealed a local LGM advance considerably less extensive than previous
322 glaciations, followed by several glacial front stabilizations at 17, 13 and 12 ka (Hughes et
323 al., 2010). Finally, cosmogenic isotope datasets based on ^{36}Cl from different mountain areas
324 across Turkey support a LGM stade between 26 and 20.3 ka, followed by several glacial

325 advances during the Lateglacial (Akçar et al., 2007; Sarikaya et al., 2009; Zahno et al.,
326 2010).

327 In summary the available dates from the Sanabria Lake glacier record support: (i) at least
328 two glacial advances close in extent (a double local MIE) during the last glacial cycle, the
329 first one prior to 33 ka and the second one during the LGM of MIS 2; and (ii) a sequence of
330 glacial front stabilizations between 19.2 and 15.4 ^{10}Be ka that is synchronous with the
331 Lateglacial evolution of other mountain glaciers in southern Europe. Glacier evolution in
332 southern latitudes is closely controlled by moisture availability and, at orbital time scales,
333 to the latitudinal shifts of climate patterns. The North Atlantic Polar Front shift towards the
334 South was more pronounced during MIS 2 than during MIS 4, pushing the prevailing
335 westerly storms more to the south and reducing the precipitation in central and northern
336 Europe accordingly (Florineth and Schlüter, 2000). The latter would explain a shorter
337 extent of glacial advances in northern Iberian mountain areas, particularly the Cantabrian
338 Mountains and the northwestern Pyrenees. Nevertheless, additional chronological data are
339 needed to test this hypothesis, especially in the Cantabrian Mountains where available
340 chronologies for the last glacial cycle are currently based on ^{14}C AMS and OSL.

341 **6. Conclusions**

342 New chronological data based on the cosmogenic nuclide ^{10}Be in the Sanabria area
343 supports a sequence of moraines formed between 19.2 and 15.4 ^{10}Be ka, interpreted as the
344 result of successive stabilizations during general retreat during the Lateglacial. This record
345 constitutes additional evidence for a glacial episode coeval with the global LGM of MIS 2
346 in SW Europe. The combination of the geomorphological observations, published ^{14}C and
347 OSL dates, and the new TCN results, suggests a double local MIE, since the local LGM
348 advance might be close in extent compared to the previous Würmian MIE stade (33 ka).

349 Our chronology correlates well with: (i) published TCN chronologies established in other
350 mountain areas of southern Europe; and (ii) palaeoclimatic reconstructions for Iberia, which
351 indicate that the coldest and driest conditions for the last 25 ka took place during the
352 Lateglacial, matching the Mystery Interval. This study demonstrates that the combination
353 of geomorphological surveys and several dating techniques can help to constrain
354 chronologies and develop more accurate palaeoglacial models, particularly in areas with
355 complex moraine systems.

356 **Acknowledgements**

357 Research funded by Spanish CICYT projects LIMNOCAL–CGL2006-13327-C04-01,
358 GRACCIE-CSD2007-0006, TOPOIBERIA-CSD2006-0041 (Consolider Ingenio Program),
359 RISKNAT-2009SGR520, and *Fundación Patrimonio Natural CyL*. L. Rodríguez-
360 Rodríguez is granted by the Severo Ochoa (FICYT–Asturias) and the FPU (Spanish
361 MEC) programs. The AMS facility ASTER (CEREGE) is supported by the INSU/CNRS,
362 the French MESR, and the CEA institute. We are grateful to M. Arnold, G. Aumaître, and
363 K. Keddarouche for the AMS measurements and to the Administration of the Sanabria
364 Natural Park for the sampling permissions.

365 **References**

- 366 Akçar, N., Yavuz, V., Ivy-Ochs, S., Kubik, P.W., Vardar, M., Shlüchter, C., 2007.
367 Paleoglacial records from Kavron Valley, NE Turkey: Field and cosmogenic
368 exposure dating evidence. *Quaternary International* 164–165, 170–183.
- 369 Allen, J.R.M., Huntley, B., Watts, W. A., 1996. The vegetation and climate of northwest
370 Iberia over the last 14,000 yr. *Journal of Quaternary Science* 11, 125–147.

371 Balco, G., 2006. Converting Al and Be isotope ratio measurements to nuclide
372 concentrations in quartz. Available at: <https://hess.ess.washington.edu> (accessed
373 April 2012)

374 Balco, G., 2010. ^{26}Al – ^{10}Be exposure age/erosion rate calculators: update of constants file
375 from 2.2 to 2.2.1. Available at: <https://hess.ess.washington.edu> (accessed April 2012)

376 Balco, G., Stone, J., Lifton, N.A., Dunai, T., 2008. A complete and easily accessible means
377 of calculating surface exposure ages or erosion rates from ^{10}Be and ^{26}Al
378 measurements. *Quaternary Geochronology* 3, 174-195.

379 Benn, D. I. Hulton, N. R. J., 2010. An ExcelTM spreadsheet program for reconstructing the
380 surface profile of former mountain glaciers and ice caps. *Computers & Geosciences*
381 36, 605-610.

382 Calvet, M., Delmas, M., Gunnell, Y., Braucher, R., Bourlès, D., 2011. Recent advances in
383 research on Quaternary glaciations in the Pyrenees. *Developments in Quaternary*
384 *Science* 15, 127-139.

385 Carrasco, R. M., Pedraza, J., Domínguez-Villar, D., Villa, J., Willenbring, J. K., 2013. The
386 plateau glacier in the Sierra de Béjar (Iberian Central System) during its maximum
387 extent. Reconstruction and chronology. *Geomorphology* 196, 83-93.

388 Clark, P. U., Dyke, A. S., Shakun, J. D., Carlson, A. E., Clark, J., Wohlfarth, B., Mitrovica,
389 J. X., Hostetler, S. W., McCabe, A. M., 2009. The Last Glacial Maximum. *Science*
390 325, 710–714.

391 Cowton, T., Hughes, P. D., Gibbard, P. L., 2009. Palaeoglaciation of Parque Natural Lago
392 de Sanabria, northwest Spain. *Geomorphology* 108, 282-291.

393 Darnault, R., Rolland, Y., Braucher, R., Bourlès, D., Revel, M., Sánchez, G., Bouissou, S.,
394 2012. Timing of the last deglaciation revealed by receding glaciers at the Alpine-
395 scale: impact on mountain geomorphology. *Quaternary Science Reviews* 31, 127-142.

396 Delmas, M., Gunnell, Y., Braucher, R., Calvet, M., Bourlès, D., 2008. Exposure ages
397 chronology of the last glaciation in the eastern Pyrenees. *Quaternary Research* 69,
398 231-241.

399 Delmas, M., Calvet, M., Gunnell, Y., 2009. Variability of Quaternary glacial erosion rates –
400 A global perspective with special reference to the Eastern Pyrenees. *Quaternary*
401 *Science Reviews* 28, 484-498.

402 Delmas, M., Calvet, M., Gunnell, Y., Braucher, R., Bourlès, D., 2011. Palaeogeography
403 and ¹⁰Be exposure-age chronology of Middle and Late Pleistocene glacier systems in
404 the northern Pyrenees: Implications for reconstructing regional palaeoclimates.
405 *Palaeogeography, Palaeoclimatology, Palaeoecology* 305, 109-122.

406 Denton, G.H., Alley, R.B., Comer, G.C., Broecker, W.S., 2005. The role of seasonality in
407 abrupt climate change. *Quaternary Science Reviews* 24, 1159-1182.

408 Denton, G.H., Broecker, W., Alley, R.B., 2006. The mystery interval 17.5 to 14.5 kyr ago.
409 In Brigham-Grette, J., Kull, C., Kiefer, T. (Eds.), *PAGES News*, 14-16.

410 Ditchburn, R. G., Whitehead, N. E., 1994. The separation of ¹⁰Be from silicates. 3d
411 Workshop of the South Pacific Environmental Radioactivity Association, 4-7.

412 Domínguez-Villar, D., Carrasco, R.M., Pedraza, J., Cheng, H., Edwards, R.L., Willenbring,
413 J.K., in press. Early maximum extent of paleoglaciers from Mediterranean mountains
414 during the last glaciation. *Scientific Reports* 3, 2034; DOI:10.1038/srep02034(2013).

415 Ehlers, J., Gibbard, P. L., 2007. The extent and chronology of Cenozoic Global Glaciation.
416 *Quaternary International* 164-165, 6-20.

417 Florineth, D., Schlüchter, C., 2000. Alpine evidence for Atmospheric Circulation Patterns
418 in Europe during the Last Glacial Maximum. *Quaternary Research* 54, 295-308.

419 García-Ruiz, J. M., Valero-Garcés, B. L., Martí-Bono, C., González-Sampériz, P., 2003.
420 Asynchronicity of maximum glacier advances in the central Spanish Pyrenees. *Journal*
421 *of Quaternary Science* 18, 61-72.

422 García-Ruiz, J. M., Martí-Bono, C., Peña-Monné, J. L., Sancho, C., Rhodes, E. J., Valero-
423 Garcés, B., González-Sampériz, P., Moreno, A., 2013. Glacial and fluvial deposits in
424 the Aragón Valley, central-western Pyrenees: Chronology of the Pyrenean late
425 Pleistocene glaciers. *Geografiska Annaler* 95A (1), 15-32.

426 Gillespie, A., Molnar, P., 1995. Asynchronous maximum advances of mountain and
427 continental glaciers. *Reviews of Geophysics* 33 (3), 311-364.

428 Hughes, P. D., Woodward, J. C., 2008. Timing of glaciation in the Mediterranean
429 mountains during the last cold stage. *Journal of Quaternary Science* 23 (6-7), 575-
430 588.

431 Hughes, P. D., Woodward, J. C., Gibbard, P. L., Macklin, M., Gilmour, M., Smith, G., 2006.
432 The Glacial History of the Pindus Mountains, Greece. *Journal of Geology* 114, 413-
433 434.

434 Hughes, P. D., Woodward, J. C., van Calsteren, P. C., Thomas, L. E., Adamson, K. R.,
435 2010. Pleistocene ice caps on the coastal mountains of the Adriatic Sea. *Quaternary*
436 *Science Reviews* 29, 3690-3708.

437 Ivy-Ochs, S., Kerschner, H., Reuther, A., Preusser, F., Heine, K., Maisch, M., Kubik, P.,
438 Schlüchter, C., 2008. Chronology of the last glacial cycle in the European Alps.
439 *Journal of Quaternary Science* 23, 559-573.

440 Jalut, G., Turu i Michels, V., Deboubat, J. J., Otto, T., Ezquerro, J., Fontugne, M., Belet, J.
441 M., Bonnet, L., Garcia de Celis, G., Redondo-Vega, J. M., Vidal-Romaní, J. R.,
442 Santos, L., 2010. Paleoenvironmental studies in NW Iberia (Cantabrian range):
443 vegetation history and synthetic approach of the last deglaciation phases in the western
444 Mediterranean. *Palaeogeography, Palaeoclimatology, Palaeoecology* 297 (2), 330-350.

445 Jiménez-Sánchez, M., Farias, P., 2002. New radiometric and geomorphologic evidence of
446 Last Glacial maximum older than 18 ka in SW European Mountains: the example of
447 Redes Natural Park, Cantabrian Mountains, NW Spain. *Geodinamica Acta* 15, 93-101.

448 Jiménez-Sánchez, M., Rodríguez-Rodríguez, L., García-Ruiz, J. M., Domínguez-Cuesta,
449 M. J., Farias, P., Valero-Garcés, B., Moreno, A., Rico, M., Valcárcel, M., 2013. A
450 review of glacial geomorphology and chronology in northern Spain: timing and
451 regional variability during the last glacial cycle. *Geomorphology* 196, 50-64.

452 Kohl, C. P., Nishiizumi, K., 1992. Chemical isolation of quartz for measurement of *in-situ*-
453 produced cosmogenic nuclides. *Geochimica et Cosmochimica Acta* 56, 3583-3587.

454 Lewis, C. J., McDonald, E. V., Sancho, C., Peña, J. L., Rhodes, E. J., 2009. Climatic
455 implications of correlated Upper Pleistocene glacial and fluvial deposits on the Cinca
456 and Gállego Rivers (NE Spain) based on OSL dating and soil stratigraphy. *Global and
457 Planetary Change* 67, 141-152.

458 Makos, M., Nitychoruk, J., Zreda, M., 2013. Deglaciation chronology and paleoclimate of
459 the Pięciu Stawów Polskich/Roztoki Valley, high Tatra Mountains, Western
460 Carpathians, since the Last Glacial Maximum, inferred from ³⁶Cl exposure dating and
461 glacier-climate modeling. *Quaternary International* 293, 63-78.

462 Moreno, A., Valero-Gracés, B. L., Jiménez-Sánchez, M., Domínguez, M. J., Mata, P.,
463 Navas, A., González-Sampériz, P., Stoll, H., Farias, P., Morellón, M., Corella, P.,

464 Rico, M., 2010. The last deglaciation in the Picos de Europa National Park
465 (Cantabrian Mountains, northern Spain). *Journal of Quaternary Science* 25 (7), 1076-
466 1091.

467 Moreno, A., González-Sampériz, P., Morellón, M., Valero-Garcés, B., Fletcher, W. J.,
468 2012. Northern Iberian abrupt climate change dynamics during the last glacial cycle:
469 A view from lacustrine records. *Quaternary Science Reviews* 36, 139-153.

470 Muñoz-Sobrino, C., Ramil-Rego, P., Gómez-Orellana, L., 2004. Vegetation of the Lago de
471 Sanabria area (NW Iberia) since the end of the Pleistocene: a palaeological
472 reconstruction on the basis of two new pollen sequences. *Vegetation History and*
473 *Archaeobotany* 13, 1-22.

474 Muñoz-Sobrino, C., Heiri, O., Hazekamp, M., van der Velden, D., Kirilova, E.P., García-
475 Moreiras, I., Lotter, A.F., 2013. *Quaternary Science Reviews* 80, 58 - 77.

476 Nishiizumi, K., Imamura, M., Caffee, M. W., Southon, J. R., Finkel, R. C., McAninch, J.,
477 2007. Absolute calibration of ^{10}Be AMS standards. *Nuclear Instruments and Methods*
478 *in Physics Research B* 258, 403-413.

479 Palacios, D., Marcos, J., Vázquez-Selem, L., 2010. Last Glacial Maximum and deglaciation
480 of Sierra de Gredos, central Iberian Peninsula. *Quaternary International* 233 (1), 16-
481 26.

482 Palacios, D., Andrés, N., Marcos, J., Vázquez-Selem, L., 2012. Glacial landforms and their
483 paleoclimatic significance in Sierra de Guadarrama, Central Iberian Peninsula.
484 *Geomorphology* 139-140, 67-78.

485 Pallàs, R., Rodés, A., Braucher, R., Carcaillet, J., Ortuño, M., Bordonau, J., Bourlès, D.,
486 Vilaplana, J.M., Masana, E., Santanach, P., 2006. Late Pleistocene and Holocene

487 glaciation in the Pyrenees: a critical review and new evidence from ¹⁰Be exposure
488 ages, south-central Pyrenees. *Quaternary Science Reviews* 25, 2937-2963.

489 Pallàs, R., Rodés, A., Braucher, R., Bourlès, D., Delmas, M., Calvet, M., Gunnell, Y.,
490 2010. Small isolated glacial catchments as priority target for cosmogenic surface
491 dating of Pleistocene climate fluctuations, SE Pyrenees. *Geology* 38, 891–894.

492 Pérez-Alberti, A., Valcárcel-Díaz, M., Martini, I. P., Pascucci, V., Andrucci, S., 2011.
493 Upper Pleistocene glacial valley-junction sediments at Pias, Trevinca Mountains, NW
494 Spain, In: Martini, I. P., French, H. M., Pérez-Alberti, A. (Eds.), *Ice-Marginal and*
495 *Periglacial Processes and Sediments*, Geological Society, London, Special Publication
496 354, pp. 93-110.

497 Rodríguez-Rodríguez, L., Jiménez-Sánchez, M., Domínguez-Cuesta, M. J., Rico, M. T.,
498 Valero-Garcés, B., 2011. Last deglaciation in northwestern Spain: New chronological
499 and geomorphologic evidence from the Sanabria region. *Geomorphology* 135, 48-65.

500 Sarikaya, M., Zreda, M., Çiner, A., 2009. Glaciations and paleoclimate of Mount Erciyes,
501 central Turkey, since the Last Glacial Maximum, inferred from ³⁶Cl cosmogenic
502 dating and glacier modeling. *Quaternary Science Reviews* 28, 2326-2341.

503 Serrano, E., González-Trueba, J. J., González-García, M., 2012. Mountain glaciation and
504 paleoclimate reconstruction in the Picos de Europa (Iberian Peninsula, SW Europe).
505 *Quaternary Research* 78, 303-314.

506 Serrano, E., González-Trueba, J. J., Pellitero, R., González-García, M., Gómez-Lende, M.,
507 2013. Quaternary glacial evolution in the Central Cantabrian Mountains (Northern
508 Spain). *Geomorphology* 196, 65-82.

509 Vieira, G., 2008. Combined numerical and geomorphological reconstruction of the Serra da
510 Estrela plateau icefield, Portugal. *Geomorphology* 97, 190-207.

511 Weninger, B., Jöris, O., 2008. A ^{14}C age calibration curve for the last 60 ka: the Greenland-
512 Hulu U/Th timescale and its impact on understanding the Middle to Upper Paleolithic
513 transition in western Eurasia. *Journal of Human Evolution* 55, 772-781.

514 Weninger, B., Jöris, O., Danzeglocke, U., 2007. CalPal-2007. Cologne Radiocarbon
515 Calibration and Palaeoclimate Research Package. Available at:
516 <http://222.calpal.de/2007> (May 2012)

517 Woodward, J. C., Lewin, J., Macklin, M.G., 1995. Glaciation, river behaviour and the
518 Palaeolithic settlement of upland northwest Greece. In Lewin, J., Macklin, M.G.,
519 Woodward, J.C., (Eds.) *Mediterranean Quaternary River Environments*, Rotterdam,
520 Balkema: 115-129.

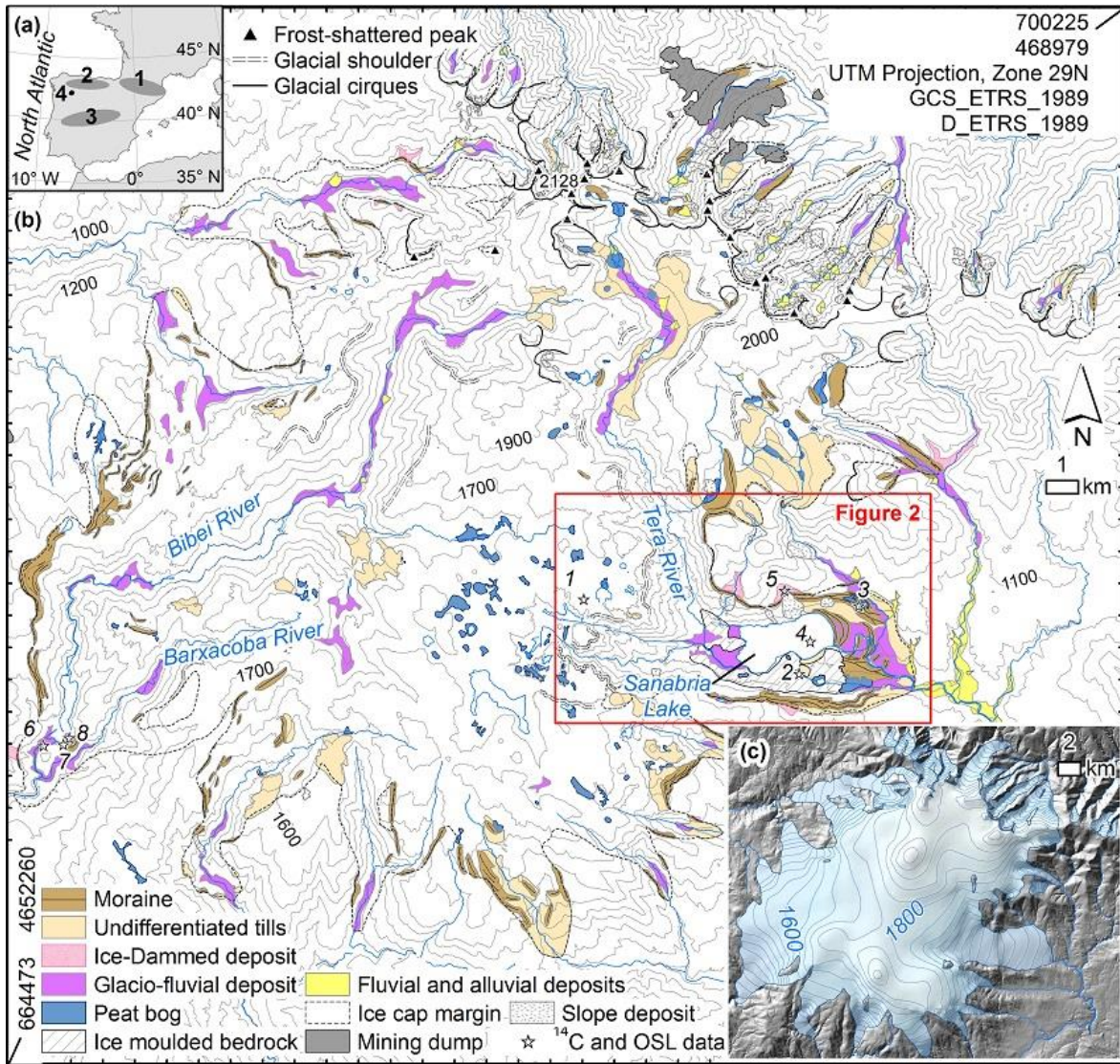
521 Woodward, J. C., Hamlin, R.H.B., Macklin, M.G., Hughes, P.D., Lewin, J., 2008. Glacial
522 activity and catchment dynamics in northwest Greece: Long-term river behaviour and
523 the slackwater sediment record for the last glacial to interglacial transition.
524 *Geomorphology* 101, 44-67.

525 Zahno, C., Akçar, N., Yavuz, V., Kubik, P. W., Schlüchter, C., 2010. Chronology of Late
526 Pleistocene glacier variations at the Uludağ Mountain, NW Turkey. *Quaternary*
527 *Science Reviews* 29, 1173-1187.

528 Zreda, M., Çiner, A., Akif Sarikaya, M., Zweck, C., Bayari, S., 2011. Remarkably
529 extensive glaciation and fast deglaciation and climate change in Turkey near the
530 Pleistocene-Holocene boundary. *Geology* 39, 1051-1054.

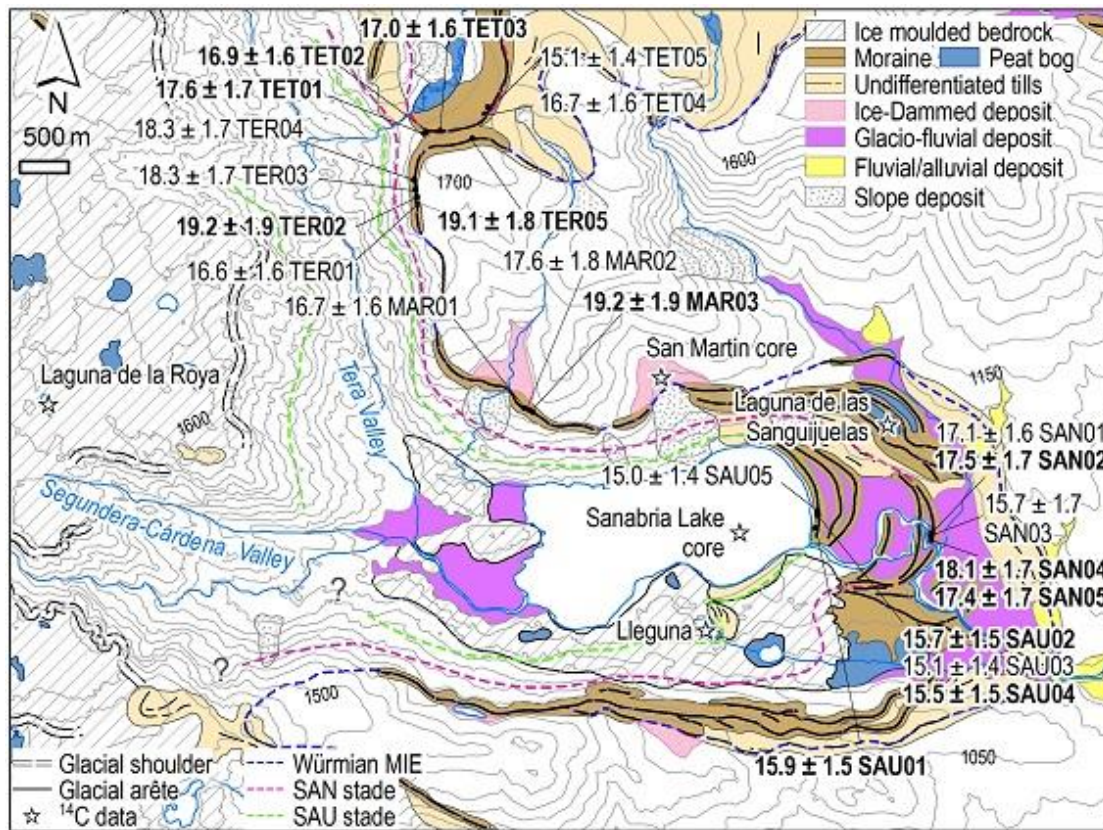
531
532
533

534 **Figure 1.** (a) Setting (1- Pyrenees, 2- Cantabrian Mts., 3- Sistema Central, 4- Trevinca
 535 Massif). (b) Geomorphological map of the Trevinca Massif, including published ages:
 536 radiocarbon data (1-5) (see also Table 1) and optically stimulated luminescence data (OSL)
 537 from Pias site (6-8; Pérez-Alberti et al., 2011). The rectangle indicates Figure 2 location. (c)
 538 Ice cap reconstruction for the local maximum ice extent (MIE).



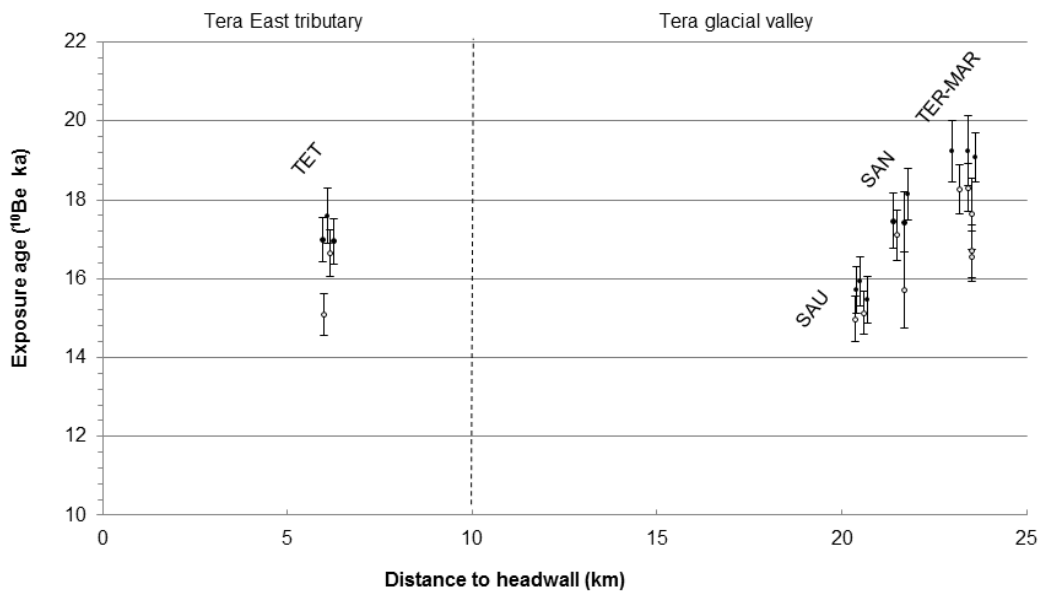
539
 540
 541
 542

543 **Figure 2.** Geomorphological map of the Sanabria Lake area showing the location of the
 544 sampled boulders and the minimum exposure ages (^{10}Be) reported in this work, expressed
 545 in ka with the analytical (1σ) and external uncertainty for age comparisons with other
 546 datasets. Dates used to calculate the minimum ages for each moraine are represented in
 547 bold.



548
 549
 550
 551
 552
 553
 554
 555

556 **Figure 3.** ^{10}Be exposure ages calculated with online CRONUS calculator (Balco et al.,
557 [2008; v. 2.2.1 updated in Balco, 2010](#)). Samples are arranged from left to right according to
558 [distance from cirque headwall or ice dome \(case of TET moraine\)](#). Black dots indicate
559 [which samples were used to derive moraine minimum exposure ages](#), while error bars
560 [indicate the analytical uncertainty \(\$1\sigma\$ \) for each sample](#). Boulder ages are tightly grouped
561 [within each moraine](#).



562
563
564
565
566

567 **Figure 4.** Examples of moraines sampled for the TCN analysis: (a) panorama of the TER
 568 moraine looking northwards, with TER01 in the foreground and the Tera valley in the
 569 background; (b) panorama of the MAR sample sites including one of the ice-dammed
 570 deposits formed behind the Sanabria Lake north lateral moraine; and (c) TET moraine
 571 panorama looking northeastward; including in the foreground the boulder where sample
 572 TET04 was collected. Boulder age uncertainties include only the analytical uncertainty.



573